Structural Design of a Wood-CFRP Wind Turbine Blade Model

Rasmus Borrmann

Flensburg University of Applied Sciences
Wind Energy Technology Institute

2016

Abstract

Because of its favorable ratio of elastic modulus to density, its particularly high fatigue resistance, and its convenient damping behavior, wood is well suited to be used for the design of wind turbine rotor blades. In contrast to synthetic composites, wood is fully recyclable. In the development towards today's wind energy technology many wooden rotor blades have been realized. A major disadvantage of the different wooden rotor blade concepts were difficulties to obtain the chosen wood products in high and reproducible quality. To overcome this disadvantage, a blade concept is proposed, that uses mass produced laminated veneer lumber (LVL) combined with spar cap reinforcements made of carbon fiber reinforced plastic (CFRP). A structural design of rotor blades with a length of 61.5 m is made for the NREL 5 MW reference wind turbine and compared with a conventional rotor blade.

Contents

1 Introduction

Conventional blade concepts involve significant manual labor, limited automation potential, and an unresolved recycling issue. In order to reduce the cost of electricity and minimize recycling difficulties a different blade concept is proposed, that consists mainly of mass-produced wood and is manufactured in an automated process.

1.1 Conventional Blade Design

Today's horizontal axis wind turbine rotor blades are designed as composite structures. Widely used composites are glass and carbon fiber in polyester or epoxy resin. The rotor blades usually consist of a beam structure integrated into an aerodynamic fairing. The internal beam structure comprises spar caps with unidirectional fibers connected by one or more shear webs. To stop the shell from buckling it is often designed as a sandwich panel with a balsa or synthetic foam core separating layers of multi-directional laminates.

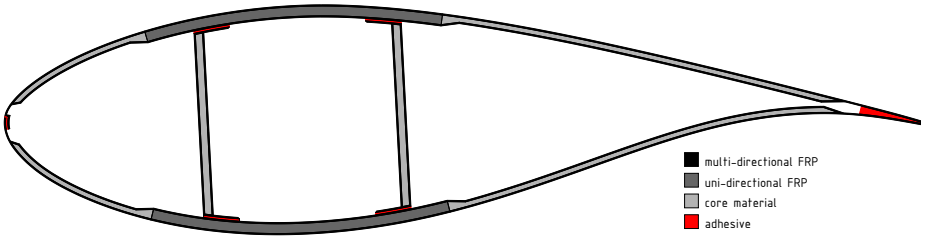

Figure 1: Cross section of a conventional blade

Most blades are built with the help of negative half shell molds. The major manufacturing approaches use either dry fiber cloth or pre-impregnated fiber mats (prepregs) that are laid into the negative molds. When dry fiber cloth is used, resin is infused through a vacuum bag. Both resin infusion and prepreg composites are typically heated inside the mold, so that the resin can harden faster. The prepreg method provides higher and more consistent glass to resin ratios, but leads to higher manufacturing costs. Shear webs and sometimes the spar caps are built in a separate process. Afterwards, the different components are joined together and cured. Finally, the surface and especially the leading and trailing edge bonds get another treatment to guarantee sufficient surface quality.

The presented blade design and manufacturing approach has proven to be eligible for modern wind turbines and differences between blade suppliers are rather small.

The process however still poses some significant difficulties. Because of the high amount of manual labor, manufacturing tolerances and safety factors are considerably high. Dependency on a skilled work force is immense. Despite ongoing efforts from the industry and the research community, the automation potential of conventional blade manufacturing processes is limited.

At present wind turbines have a design life of 20 years. Though the lifetime of future wind turbines especially in the offshore industry might be extended, recycling of wind turbine components will become increasingly important. Nowadays, there is no way to recycle rotor blades made of synthetic composites. The only potential lies in down-cycling the materials to be used for instance as filling material in road constructions.

New approaches in blade manufacturing involve modular blades for better logistics and integral blade shells, that don't need to be bonded at the edges. Another focus is on so called smart blades that reduce loads by an adaptive aerodynamic behavior.

1.2 History of Wooden Blades

Blades of wind turbines need to provide aerodynamic performance and structural integrity at low weight and cost. For a beam structure that is mainly subjected to bending loads and limited by its cross section's dimensions, the ratio of young's modulus to density can be a good indicator for a material's technical suitability, whereas the ratio of young's modulus to material cost gives an indication on the economic feasibility. Wood has good ratios of strength to density and young's modulus to density and very good ratios of strength to cost and young's modulus to cost [1]. While the absolute values for the young's modulus of wood is comparably low, the density specific modulus (E/ρ) of wood (parallel to the grain) can be higher than the density specific modulus of glass fiber reinforced plastic (GFRP). The highest density specific modulus of all materials used for rotor blade construction is found for carbon fiber reinforced plastic (CFRP).

Blades are subjected to cyclic loading caused by rotation, turbulent winds, and turbine control. As such, to withstand load cycle numbers in the range of $n = 10^8$ the blade's materials need to have sufficient fatigue strength. Compared to synthetic composites and metals, wood has by far the best fatigue characteristics. Wood materials have a long tradition for construction purposes and the ways of wood processing are versatile. Automation is well-established in the various steps of wood processing. In terms of availability and price, wood products can be expected to have competitive advantages against synthetic composites. Recycling of wood structures is possible.

On the way to modern wind turbine technology, various approaches of using wood for wind turbine blades have been analyzed. Some have been implemented for serial production of several thousand blades.

Even today, blades for small wind turbines and sporting airplanes are built from wood because of its high fatigue strength and favorable damping characteristics. These rotors are usually constructed as solid wooden bodies and are often manufactured in a computerized milling process. Because solid bodies have high masses per length, this approach is not suitable for larger rotor blades. Also, the loading of small rotors with high revolution speeds differs greatly from larger rotor blades, which are mainly subjected to bending loads.

Another approach to wooden rotor blades has been traditional wood construction, where a framework of ribs and stringers is covered with planks. Research on this design has been conducted at the Danish Nibe-B test turbine, but stopped short because of anticipated durability problems in light of the more-promising wood epoxy alternative [2]. Wood epoxy blades were widely inspired by boat construction techniques and were first realized by the Gougeon Brothers [3]. In contrast to the traditional wood construction, the wood is fully embedded in resin by wet layup of impregnated wood veneers. This preserves the good fatigue characteristics while preventing the wood from moisture ingress. Between the years 1979 and 1993 Gougeon Brothers produced about 4,300 blades with lengths between $l = 3\,\mathrm{m}$ and $l = 21\,\mathrm{m}$. With the same design NEG Micon produced blades for the turbine NM 64C/1500 with a diameter of $D = 64\,\mathrm{m}$. The resin content used in the wood composite was about 20%.

Another approach combines wood with carbon fiber reinforcements. Here the blade shell is produced by vacuum infusion of birch wood together with pultruded strips of CFRP. This procedure was introduced by NEG Micon, later acquired by Vestas. For multi-directional strength and to protect the blade from moisture ingress the blades were covered with a layer of GFRP. Blades of this design are characterized by high stiffness stability and particularly good damping behavior.

The newest wooden blade concept is based on bamboo as spar cap material. The concept was presented in the Wind Turbine Blade Manufacture 2014 conference. LZFRP produced a set of bamboo blades with $l = 40\,\mathrm{m}$ length for a 1.5 MW turbine. Bamboo blades have not reached readiness for start of production because of problems with the procurement of adequate bamboo products and high variances of the material's mechanical properties. Today, large rotor blades are not made out of wood, although wood is recognized for its environmental attractiveness. The main reasons for not using wood are difficulties to obtain reproducible, high quality and a comparably low absolute elastic modulus [4].

Table 1: Comparison of wood blade designs

blade design	application	materials	manufacturing
solid body	small wind turbines, propellers: $> 10,000$ blades	solid wood, glued-laminated timber, laminated veneer lumber	direct milling/ sanding
conventional wood construction	test turbine Nibe-B with $D = 40\,\mathrm{m}$	solid wood, ply wood	planking of framework
wood wet layup	WT with $D \leq 64\,\mathrm{m}$: $> 4,300$ blades	wood veneers, glass fiber cloth, epoxy resin	wet layup in negative mold, vacuum compression, thermal curing
wood CFRP infusion	WT with $D \leq 82\,\mathrm{m}$: $> 8,000$ blades	wood strips, wooden veneers, CFRP strips, glass fiber cloth, epoxy resin	vacuum-infusion in negative mold, thermal curing
bamboo infusion	test turbine with $D = 82\,\mathrm{m}$	bamboo strips, glass fiber cloth, epoxy resin	vacuum-infusion in negative mold, thermal curing

1.3 Structural Design Approach

The here presented blade concept aims to overcome the automation limits of conventional blades and previous wooden blade concepts. Another key issue is to use standardized wood products of good availability.

Because of its high strength and stiffness characteristics as well as low parameter deviations, laminated veneer lumber (LVL) is preferred as the main constructive material. Through the orientation of the veneers, the anisotropic material characteristics can be controlled from unidirectional at the spar cap regions to multi-directional at the shear web. LVL is produced in a highly industrialized process from different kinds of wood and is available as boards, beams and panels of various dimensions.

To reduce blade weight and to realize larger blade sizes, it is destined to use CFRP for spar cap reinforcement. Because of the similar breaking elongation of CFRP and wood, the two materials can be combined efficiently.

To overcome the previously mentioned automation limits, the manufacturing process shall be disassociated from negative molding. Instead, the blade shape shall be realized by a direct, computerized numerical controlled (CNC) milling process, for which LVL is well-suited. For this purpose, the blank of a rotor blade has to be constructed from the provided wood products. The occurring additional cuttings costs must be compensated by a low material price. Potentially, CFRP reinforcements could be joined with the wood body later. Various options seem to be possible, ranging from prepregs to the use of pultruded elements. Sketches of the structural design approach and of a potential manufacturing process are shown in figure 2 and figure 3.

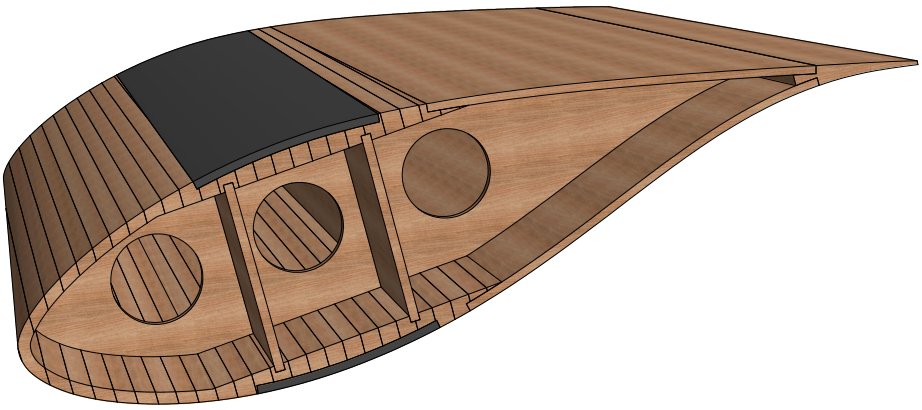

Figure 2: Cross section of a wood-CFRP blade

1.4 Objective

This work's objective is to do a structural design for a multi-megawatt onshore blade. Due to its broad academic usage and its information availability,

the NREL 5 MW turbine [5] is taken as reference turbine. The blade shall be compared to a conventional blade for the same turbine with regard to elastic properties and bill of materials. Resor [6] defined a conventional blade model for this turbine in detail. This blade model shall be used as a reference blade. To limit higher loads on other parts of the wind turbine, allowable overall blade mass is limited to 105% of the reference blade mass.

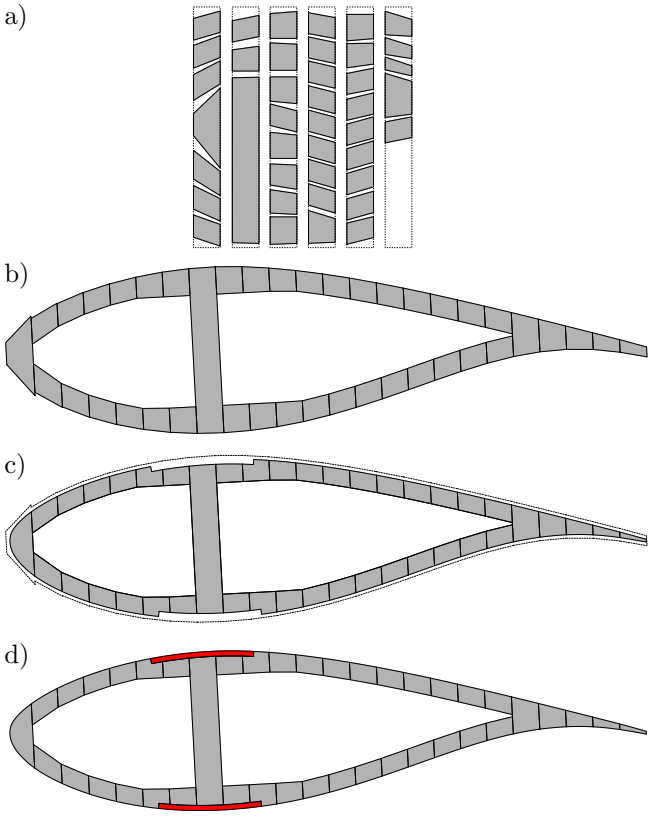

Figure 3: Manufacturing process: **a)** contour milling of lamellas, **b)** construction of blade plank, **c)** milling of blade geometry, **d)** insertion of spar cap

2 Design Method

The structural blade design is done in an iterative process that includes aero-servo-elastic wind turbine simulation. Ultimate and fatigue loads of rotor blades are the result of the interaction of aerodynamics, elastic behavior of the components and the control of a wind turbine.

Figure 4 illustrates the design process. In the initial step, the rotor blade structure is defined at various cross sections by a number of geometrical and material parameters. In the next step, a beam model of the blade is derived from the structural input. The beam model is characterized by the stiffness and mass properties of the cross sections. A simulation of various design load cases is

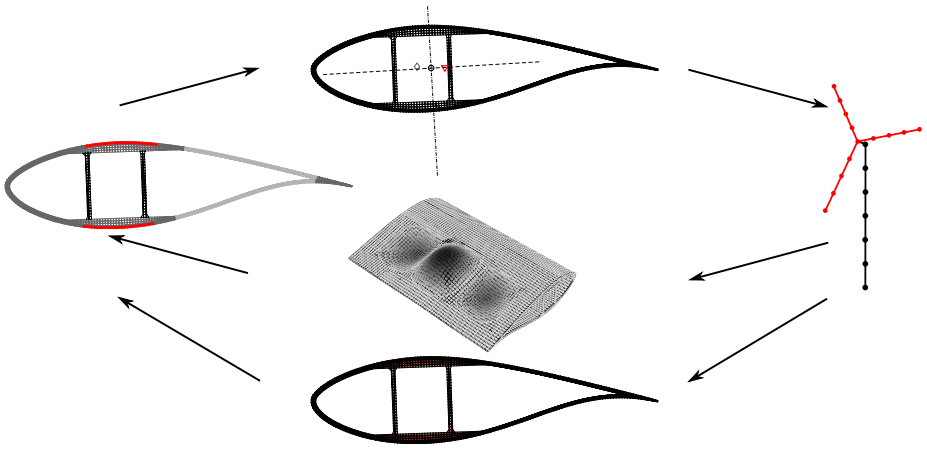

Figure 4: Design framework

carried out in which ultimate and fatigue loads are extracted from the resulting time series. Subsequently, the rotor blade structure is analyzed for ultimate strength, fatigue strength, stability and deflection. In the following step, the initial input parameters are adapted and the process is iterated until all design criteria are met.

2.1 Surface Geometry

It would be beneficial to design the aerodynamic surface together with the internal structure and material composition. This exceeds the scope of this work. Instead, the geometry is taken from the conventional reference blade.

The surface geometry is taken unchanged from Resor [6]. Resor created the outer surface of his reference blade model from the geometrical information that is given for the NREL 5 MW reference wind turbine [5]. The NREL study provides geometrical information for 17 spanwise locations. The purpose is to describe the blade's aerodynamic properties for blade element momentum theory and not to provide a detailed geometrical description. For his structural analysis, Resor complemented the 17 radial stations by interpolating 21 profile shapes. The resulting geometry can be seen in figure 5.

The structural model does not go into detail in representing the root and tip geometry as it would be needed for computational fluid dynamic analysis. With thickness to chord ratios of 40.5% to 18.0% the NREL blade uses thick profiles when compared to a low power density blade. This supports structural efficiency, because the material can be placed further from the flapwise elastic axis.

2.2 Internal Structure

The internal structure of the blade model is designed as a wooden shell that is stiffened by wooden shear webs and spar caps made of unidirectional CFRP.

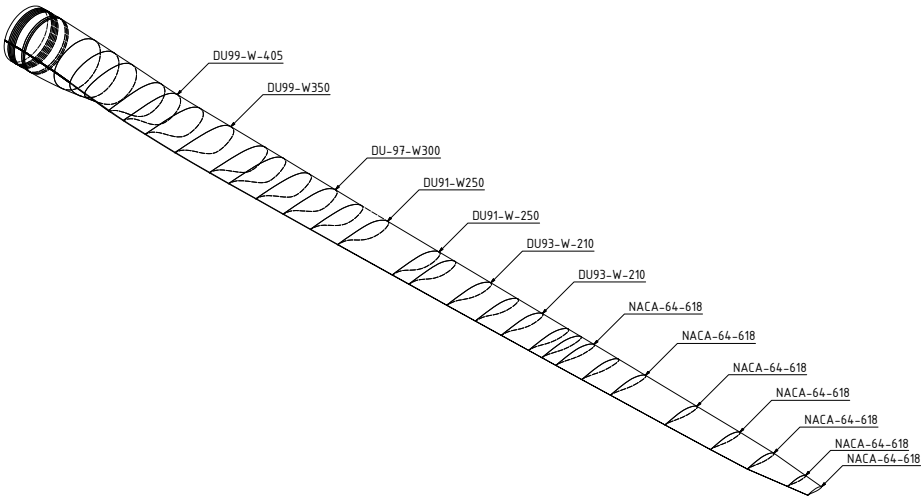

Figure 5: Rotor blade geometry

The internal structure is specified at the same 38 radial stations as is done for the reference blade.

The two-dimensional cross section layout is characterized by various geometrical parameters, defining four areas of homogeneous material characteristics as shown in figure 6. Glued connections, veneers or CFRP layers as shown in the structural concept (figure 2) are not considered individually. Instead, regions are modeled as one homogeneous part of LVL. For an illustration of the cross section parametrization see figure 7.

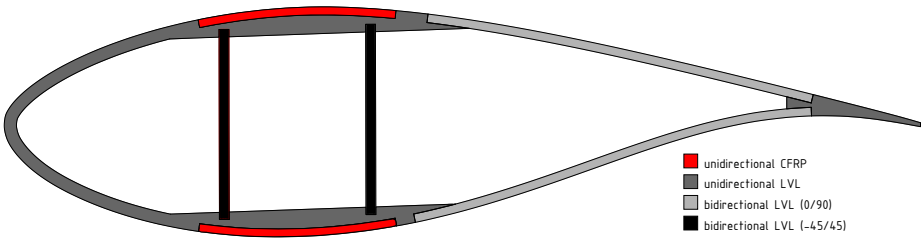

Figure 6: Internal structure

The wooden shell can be designed with a different wall thickness for leading and trailing edge regions. It is enforced by an increased wall thickness in the region of the spar caps to increase bending stiffness. Next to the various thicknesses the shell is parametrized by the orientation of the spar enforcement to the chord line.

The model allows for an arbitrary number of shear webs. The shear webs are characterized by their thickness, position on chord line, and orientation to chord line.

The spar caps are parametrized by width (given as radian measure) and thick-

ness. The position is defined by the spar caps' center line to chord line angle and the intersection point of the two lines.

The model does not represent details like the connection of the shear webs to the shell and the trailing edge joint.

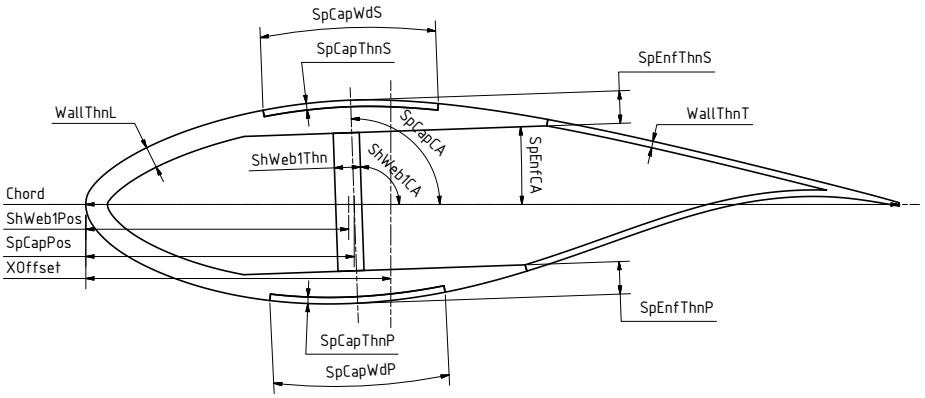

Figure 7: Cross section parametrization

Chord	Chord length.
PitchAxis	Position of pitch axis.
ShWeb2CA	Shear web to chord line angle.
ShWebPos	Shear web position as fraction of chord length.
ShWebThn	Shear web thickness.
SpCap2CA	Spar cap center axis to chord line angle.
SpCapPos	Spar cap position as fraction of the chord length.
SpCapThnP	Spar cap thickness on pressure side.
SpCapThnS	Spar cap thickness on suction side.
SpCapWdP	Spar cap width on pressure side.
SpCapWdS	Spar cap width on suction side.
SpEnf2CA	Spar enforcement to chord line angle.
SpEnfThnP	Spar enforcement thickness on pressure side.
SpEnfThnS	Spar enforcement thickness on suction side.
WallThnL	Wall thickness at leading edge.
WallThnT	Wall thickness at trailing edge.

For manufacturing purposes a constant spar cap width of 800 mm is chosen. The spar cap center axis is orientated perpendicular to the chord line for each cross section. The spar caps are approximately placed at the maximum thickness of the airfoil.

For manufacturing purposes the shear web should not be twisted. The orientation of the shear web is fixed in the blade coordinate system and corrected by the aerodynamic twist angle for each cross section.

No hardware for the blade root to hub connection is considered for this model.

2.3 Material Parameters

The blade is designed with the use of three materials: laminated veneer lumber with unidirectional layers (LVL Uniax), laminated veneer lumber with bidirectional layers (LVL Biax), and carbon fiber reinforced plastic with unidirectional fiber orientation (CFRP Uniax).

2.3.1 Laminated Veneer Lumber

LVL is an orthotropic material, which means the material properties differ along the longitudinal, tangential and radial axis. Beerschoten et al. [7] have developed a full constitutive model for Radiata Pine LVL using digital image correlation technique. For the coordinate system used see figure 8.

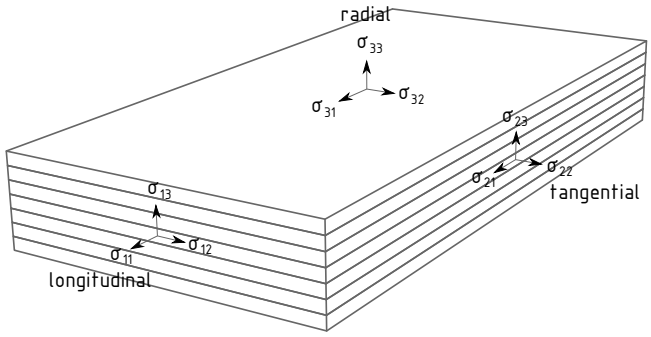

Figure 8: LVL coordinate system

From the engineering constants summarized in table 2 it can be seen that the elastic modulus in fiber direction is about factor 30 of the elastic modulus perpendicular to the fibers, while the elastic properties in tangential and radial direction are close to each other.

Table 2: Measured elastic properties of Radiata Pine LVL [7]

	E_{11} MPa	E_{22} MPa	E_{33} MPa	G_{12} MPa	G_{13} MPa	G_{23} MPa	ν_{12} -	ν_{13} -	ν_{23} -	ρ kg/m^3
LVL	12157	426	371	856	901	96	0.59	0.48	0.22	581

For this model four additional LVL products with longitudinal layers are studied and compared with LVL from Radiata Pine. The product Baubuche is made of beech, the remaining three products are made of pine and spruce. The material properties were taken from the manufacturers' declarations of performance.

Table 3 shows that LVL material properties differ depending on the processed kind of wood. Beech LVL has higher elastic moduli and shear moduli and higher ultimate strength than LVL made of soft wood. The density of beech LVL is higher than the density of soft wood LVL. Material properties also differ for the same type of wood. Different properties can result from differences in the process of LVL production, such as the material compression or the used glue.

Table 3: Comparison of different LVL products

	E_{11}	G_{13}	$\sigma_{11,t}$	$\sigma_{11,c}$	τ_{13}	ρ	E_{11}/ρ	$\sigma_{11,t}/\rho$
LVL 11 [8]	12157*	901*	30	45	6	581*	20.92	60.24
Baubuche S [9]	16800	760	60	69	8	800	21.00	75.00
Steico LVL R [10]	14000	500	36	40	4.6	510**	27.45	70.59
Steico LVL Rs [10]	15600	500	42	56	5.2	584**	26.70	71.87
Kerto-S [11]	13800	600	35	35	4.1	510	27.06	68.63

*values from table 2
**values estimated from characteristic density

Another reason for diverging properties can be differences in the growing area and growing speed of the wood and the presorting of the material.

The five LVL products are compared with respect to the specific longitudinal modulus and specific longitudinal tensile strength.

Steico LVL R is chosen for this structural blade model because it has the highest specific longitudinal modulus. Since the manufacturer does not provide a full constitutive model for this material, the missing inputs are estimated using Radiata Pine LVL as a reference. The missing elastic moduli are scaled with the reference material's ratios of tangential to longitudinal elastic modulus and radial to longitudinal modulus respectively. The missing shear moduli are scaled with the reference material's ratios of tangential to longitudinal shear modulus and radial to longitudinal shear modulus respectively. Poisson's ratios are chosen identical to the reference material.

Next to the properties of LVL with longitudinal layers, information about the properties of LVL with crosswise layers is needed. Manufacturer documentation is only available for LVL with less than 50% crosswise layers and thus cannot be taken here.

Instead, an LVL is assumed for this blade model that consists of a symmetric layup of alternating layers with fiber orientation of +45°and -45°. Another LVL is assumed that consists of a symmetric layup of alternating layers with fiber orientation of 0°and 90°. The in-plane elastic properties are derived using classical lamination theory. As a simplification, the out-of-plane properties are not computed but chosen identical to the lower out-of-plane value of the unidirectional LVL. The density is assumed to be the same as for the unidirectional LVL.

Table 4: Elastic properties of LVL

	E_{11} MPa	E_{22} MPa	E_{33} MPa	G_{12} MPa	G_{13} MPa	G_{23} MPa	ν_{12} -	ν_{13} -	ν_{23} -	ρ kg/m^3
LVL Uniax	14000	491	427	500	526	56	0.59	0.48	0.22	510
LVL Biax (-45/45)	1768 *	1768 *	427	3251 *	56	56	0.77 *	0.22	0.22	510
LVL Biax (0/90)	7323 *	7323 *	427	500 *	56	56	0.04 *	0.22	0.22	510

*calculated with classical lamination theory

2.3.2 CFRP

Material properties for unidirectional CFRP are obtained from the reference blade model [6].

Table 5: Elastic properties of CFRP

	E_{11} MPa	E_{22} MPa	E_{33} MPa	G_{12} MPa	G_{13} MPa	G_{23} MPa	ν_{12} -	ν_{13} -	ν_{23} -	ρ kg/m^3
CFRP Uniax	114500	8390	8390	5990	5990	5990	0.27	0.27	0.27	1220

2.4 Beam Elastic Properties

For this structural blade design, a modal analysis is conducted for load estimation. The beam model of the blade is limited to three degrees of freedom: the first and second flapwise mode and the first edgewise mode.

Therefore the elastic properties for each cross section are needed. In a next step, the mode shapes and natural frequencies are computed.

For the computation of cross section stiffness properties the program BECAS [12] is used. BECAS (BEam Cross section Analysis Software) is an open source software distributed by the Technical University of Denmark (DTU).

BECAS calculates stiffness properties for arbitrary cross section geometries from finite elements. It is capable of handling anisotropic materials in any orientation and accounts for geometrical and material induced coupling.

BECAS is supplemented by tools for the generation of two dimensional finite element meshes (see Airfoil2becas and Shellexpander). These tools are not suitable for the described cross section layout, because they cannot account for the various geometrical parameters. Input for BECAS is instead generated by PASEM (Parametrized Cross Section Mesher), a Python script that was developed at WETI for this specific purpose. Based on the geometrical parameters defined in section 2.2, the relevant profile geometry, and additional parameters that define the respective material orientation, a two-dimensional mesh is generated and provided in the format required by BECAS. PASEM allows for circumferential and radial specification of the element size.

For the reduced order beam model, only the edgewise and flapwise stiffness and the mass density computed by BECAS is needed. Stiffness properties are given with respect to the elastic axes of the cross section. The elastic axes do not necessarily match the chord line and its perpendicular axis. Figure 9 shows the geometry definition and discretization as output of PASEM for an exemplary cross section at 50% blade length. Figure 10 shows the elastic axes and relevant centers of the same cross section as output of BECAS.

Natural frequencies and mode shapes are computed using the program BModes provided by NREL [13]. BModes uses flapwise and edgewise stiffness together

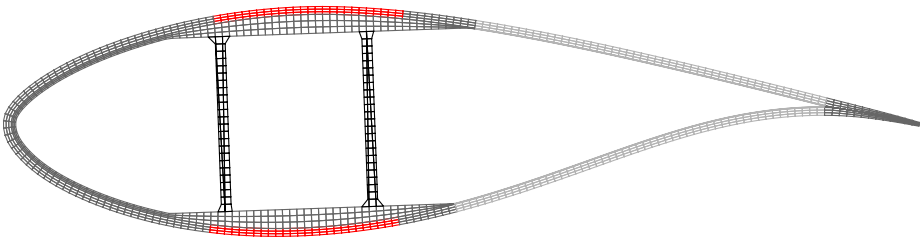

Figure 9: Cross section mesh generated by PASEM

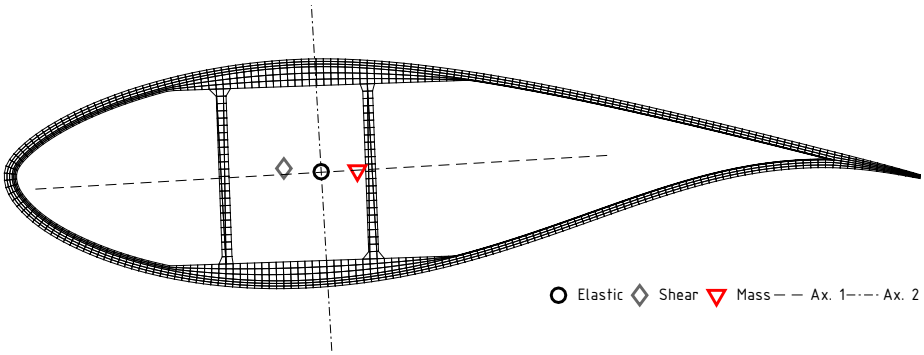

Figure 10: Centers and axes calculated by BECAS

with the mass density as input. Natural frequencies and mode shapes are computed for normal operation with a rotational speed of 12.1 min^{-1}. The mode shapes are normalized to a blade length of 1 and a tip deflection of 1. The mode shapes are then approximated with a polynomial of degree six. Figure 11 shows normalized shapes for the first and second flapwise mode. Structural damping parameters are taken from the reference blade

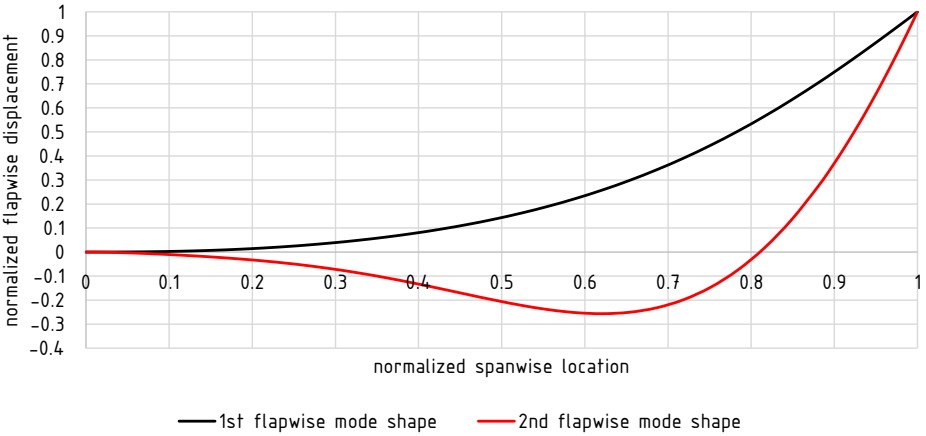

Figure 11: Flapwise mode shapes

2.5 Load Calculation

Load calculation is performed in accordance with Resor [6], using the programs FAST [14] together with TurbSim [15] and IECWind.

Design load cases (DLC) are specified in the design standard for wind turbines, IEC 61400-1 [16]. Onshore conditions according to wind class IEC IB are assumed.

For the certification of a wind turbine, a huge set of DLC has to be simulated. For this conceptual study a reduced set of DLC is being considered, including power production under various turbulent and deterministic wind conditions and parking situations with occurrence of extreme wind situations and yaw misalignment. These load cases have been chosen by Resor because they are regarded the design drivers for most wind turbine blades. All considered DLC are summarized in table 6.

Table 6: Design load cases

DLC	wind condition	γ_f	Seeds	Time	n
1.1	NTM v_{ave} from 5 m/s to 23 m/s (steps of 2 m/s)	1.35	6	30 s + 600 s	60
1.2	NTM v_{ave} from 5 m/s to 23 m/s (steps of 2 m/s)	1.35	6	30 s + 600 s	60
1.3	ETM v_{ave} from 5 m/s to 23 m/s (steps of 2 m/s)	1.35	6	30 s + 600 s	60
1.4	ECD+R-2.0 ECD+R ECD+R+2.0 ECD-R-2.0 ECD-R ECD-R+2.0	1.35	-	30 s + 100 s	6
1.5	EWS v from 3 m/s to 25 m/s positive and negative shear	1.35	-	30 s + 100 s	24
6.1	EWM50 yaw angle from $-15°$ to $15°$ (steps of $5°$)	1.35	-	30 s + 100 s	7
6.3	EWM01 yaw angle from $-30°$ to $30°$ (steps of $5°$)	1.35	-	30 s + 100 s	13
				33.3 h	230

Turbulent wind fields (DLC 1.1 to DLC 1.3) are generated with a resolution of 43 times 43 grid points on an area of 130 m times 130 m and a simulation time step of 0.5 s. Kaimal is chosen as a turbulence model. TurbSim [15] is used for the generation of turbulent wind fields.

Deterministic wind files are generated using the program IECWind that is also provided by NREL.

The load calculation is conducted with FAST and the standard onshore configuration of the NREL 5 MW reference wind turbine with a simulation time step of 0.0125 s. The blade input file is the only structural input being changed.

Some settings of Resor's load calculation have not been published. Examples are the resolution of the turbulent wind field and the initial blade azimuth angle

and the initiation time. Additionally, different program versions have been used. To check the plausibility of the chosen configuration for load estimation, the blade root loads are calculated with the use of Resor's reference blade. A comparison to the loads calculated by Resor shows that extreme loads occur with one exception under identical wind conditions and that deviations are within an acceptable range.

Table 7: Load validation

DLC	Myb / kNm		f / %	simulation	
	Resor*	Borrmann**		Resor	Borrmann
1.2	15310	16180	5.68	15 m/s	15 m/s
1.3	17990	17870	-0.67	19 m/s	19 m/s
1.4	18120	18400	1.55	ECD-R	ECD-R
1.5	13360	14460	8.23	11 m/s	11 m/s
6.1	22740	21580	-5.10	+15°	+15°
6.3	15630	16790	7.42	+20°	+25°

*FAST v7.01a, TurbSim v1.06.00, IECWind v5.01.02
**FAST v8.10, TurbSim v1.06.00, IECWind v5.01.02

Loads (forces and moments) are recorded for ten spanwise locations (so called blade gage nodes). The positions are shown by the highlighted cross sections in figure 12.

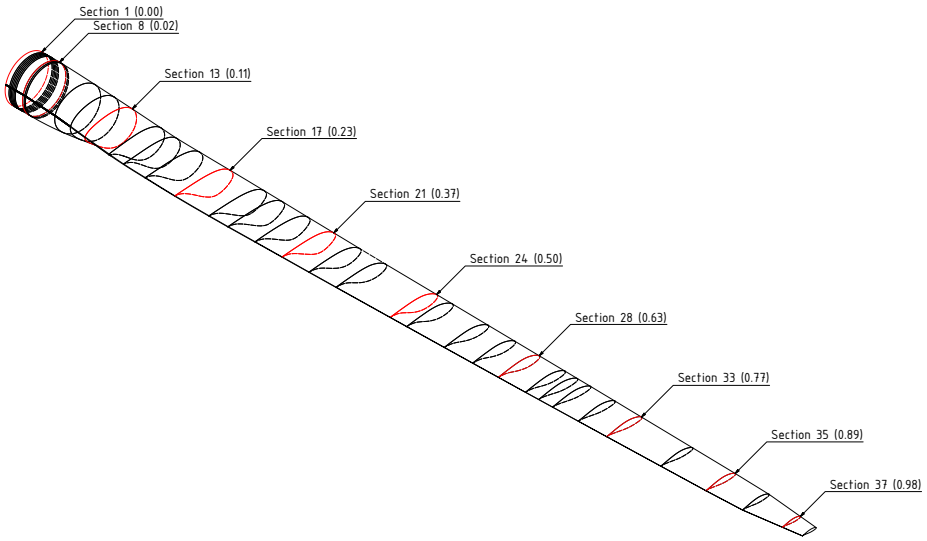

Figure 12: Blade gage nodes

2.6 Ultimate Strength Analysis

In every situation the resistance of the blade has to be at least as high as the occurring load. The ultimate strength analysis is conducted according to IEC

61400-1 and uses the partial safety factor concept:

$$\gamma_f F_k \leq \frac{1}{\gamma_m \gamma_n} f_k \tag{1}$$

F_k Characteristic value of the loads.
f_k Characteristic values of the material properties.
γ_f Partial safety factor for the loads.
γ_m Partial safety factor for the material properties.
γ_n Partial safety factor for the consequence of failure.

This can be rewritten as:

$$\frac{\gamma_f \gamma_m \gamma_n F_k}{f_k} \leq 1 \tag{2}$$

The international standard for timber constructions (EC 5) defines modification factors that depend on the time of loading and the moisture content of the material. Due to the very short occurrence time of extreme loads, a favorable value of $k_{mod} = 1.10$ is applied.

$$R_d = k_{mod} \frac{R_k}{\gamma_m} \tag{3}$$

R_d Design value of load-carrying capacity.
R_k Characteristic load-carrying capacity.
k_{mod} Modification factor for duration of load and moisture content.

In this analysis the different factors of both standards are combined for wood, ensuring that the minimum safety factor according to IEC 61400-1 is not underrun. Equation 4 represents the material utilization for ultimate strength.

$$\frac{\gamma_f \gamma_m \gamma_n F_k}{k_{mod} f_k} \leq 1 \tag{4}$$

Table 8: Safety factors for ultimate strength analysis

safety factor	value	standard	alt. value	standard
γ_f	1.35	IEC 61400		
γ_m	1.3	IEC 61400	1.0	EC5
γ_n	1.10	IEC 61400		
k_{mod}	1.10	EC5		

Ultimate loads are extracted from the various time series using the program MExtremes [17]. An extreme event table comprises the maxima and minima of the six load components and the maximum magnitude of the resulting transverse force and the maximum magnitude of the resulting bending moment. For each extreme load the simultaneous load components are given. Extreme event tables are generated for all ten blade gage nodes.

Table 9: Extreme event table

		F_x kN	F_y kN	F_z kN	M_x kNm	M_y kNm	F_z kNm	F_{xy} kN	M_{xy} kNm
F_x	min	-697	50	-270	927	-20480	489	699	20500
	max	704	-163	-276	4814	20453	-563	723	21011
F_y	min	496	-374	842	9855	18320	-367	621	20802
	max	52	314	930	-7480	1507	-145	318	7631
F_z	min	492	1	-295	2568	20966	-471	492	21122
	max	198	-35	1501	576	3299	-219	201	3349
M_x	min	200	302	1145	-7840	5177	-266	362	9396
	max	492	-374	830	9885	18050	-365	618	20579
M_y	min	-663	63	-271	802	-21735	749	666	21750
	max	659	-106	-275	5742	26244	-661	668	26865
M_z	min	657	-112	-276	5894	26217	-664	666	26871
	max	-662	64	-270	772	-21708	751	665	21722
F_{xy}	min	686	-362	815	9393	25201	-373	776	26895
M_{xy}	max	686	-362	815	9393	25201	-373	776	26895

Table 9 shows exemplary the extreme event table for the root section. All loads are given in the local chord coordinate system and include safety factors.

Material resistance is described as strain to failure. No distinction is made between tensile and compressive strain to failure. In the absence of more detailed information for LVL, axial strain to failure values are derived by dividing the lower of compressive and tensile strength in fiber direction by the elastic modulus in fiber direction. Shear strain to failure values are derived by dividing the lowest shear strength given by the respective shear modulus. Values for CFRP are derived by calculating the lower of compressive and tensile strength in fiber direction by the respective elastic modulus.

Table 10: Material strain to failure

	axial strain to failure %	shear strain to failure %
LVL Uniax	0.257	0.640
LVL Biax	0.257	0.640
CFRP Uniax	0.914	0.914

Resulting strains and stresses are calculated in BECAS for each 2D element and each of the 14 extreme events by applying the full load vector to the respective cross section.

2.7 Fatigue Strength Analysis

Both CFRP and wood are known for high fatigue resistance. Therefore fatigue is not expected to be a dimensioning criterion. A simplified method is used for fatigue strength analysis. To facilitate comparison to the reference blade, fatigue loads are expressed as damage equivalent loads (DEL).

Fatigue strength analysis is performed by extrapolating the simulated time series to 20 years of turbine operation. Only DLC 1.2 is considered for fatigue loads since normal operation is the most relevant fatigue load condition. Simulations

at different wind speeds are weighted with a Weibull-distribution with a shape factor of 2. Fatigue loads are given as the one side amplitude of DEL of 10^7 cycles at zero mean. DEL are determined for edgewise and flapwise bending moments at all ten spanwise stations based on the Palmgren-Miner's summation rule. The fatigue load analysis is performed with the program MLife [18] according to the following relation.

$$DEL^{Life} = \left(\frac{\sum_j \sum_i n_{ji}^{Life} (L_{ji}^R)^m}{n^{Life,eq}} \right)^{\frac{1}{m}} \tag{5}$$

DEL^{Life}	Lifetime damage equivalent load without Goodman correction.
n^{Life}	Extrapolated damage count for cycle i and time-series j.
L^R	Load range for cycle i and time-series j.
m	Wöhler exponent.
$n^{Life,eq}$	Lifetime equivalent counts.

For CFRP a slope parameter of $m = 14$ is assumed according to the GL Guideline for the certification of wind turbines [19] and in accordance with the reference blade.

Neither the IEC nor the GL guidelines give slope parameters for wood. Due to the bending loads and the beam structure of the wind turbine blade, the outer wooden parts experience predominantly tensile and compressive loading. Thus it is important to know the fatigue properties of wood in tension and compression.

When the first laminated wood wind turbine blades were designed, Bonfield and Ansell [20] conducted fatigue tests on specimen that were made of Khaya Ivorensis veneers laminated with epoxy resin and on specimen that were made of Douglas Fir veneers laminated with epoxy resin.

The tests show that the fatigue behavior of wood is highly dependent on the ratio of maximum to minimum stress, R. Tests were conducted for all tensile ($R = 10$), mixed tensile-compressive ($R = -1$, $R = -2$, $R = -10$) and all compressive ($R = 10$) loading. Reversed loading ($R = -1$) showed to be the most critical.

The data points for Khaya Ivorensis at reversed loading ($R = -1$) are used to estimate a slope parameter for LVL that is compatible with the DEL concept. Since the most loads are either all tensile or all compressive this can be considered a conservative estimation. A regression fit for the data points gives a Wöhler exponent of $m = 18$.

Table 11 exemplary gives the DEL at the root section for Wöhler exponents of $m = 14$ and $m = 18$.

Each cross section is loaded in BECAS with its respective combination of the DEL for edgewise and flapwise bending moments. The resulting normal stress

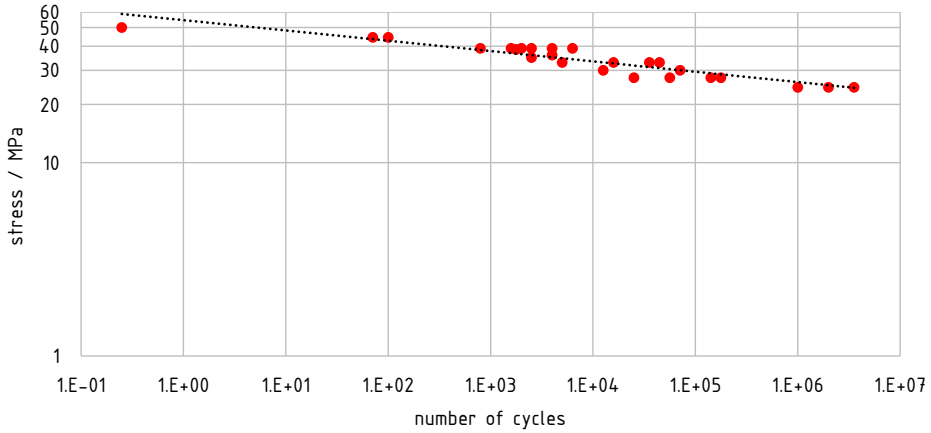

Figure 13: S-N-Curve for wood (Khaya Ivorensis)

Table 11: DEL at root section

	Mxb kNm		Myb kNm	
	$m = 14$	$m = 18$	$m = 14$	$m = 18$
section1	4862	4741	5886	6225

should always be lower than the allowable stress according to the following relation:

$$\gamma_f F_k \leq \frac{f_k}{\gamma_m \gamma_n} \tag{6}$$

This leads to the following material utilization for fatigue load:

$$\frac{\gamma_f \gamma_m \gamma_n F_k}{f_k} \leq 1 \tag{7}$$

Safety factors are applied according to IEC 61400-1 and summarized in table 12.

Table 12: Safety factors for fatigue

safety factor	value	standard	alt. value	standard
γ_f	1.0	IEC 61400		
γ_m	1.2	IEC 61400	1.0	EC5
γ_n	1.15	IEC 61400		

The fatique resistance of the different materials at $n_{ref} = 10^7$ cycles is derived according to equation 8 and summarized in table 13.

$$S = CN^{(-\frac{1}{m})} \tag{8}$$

S Resistance.
C Ultimate resistance.
N Number of cycles.

Table 13: Material resistance

	m -	C MPa	$S(n_{ref})$ MPa
LVL Uniax	18	36	14.70
LVL Biax (-45/45)	18	4.55	1.86
LVL Biax (0/90)	18	18.83	7.69
CFRP Uniax	14	1047	331

2.8 Stability

Stability analysis is conducted according to the approach that was applied for the design of the DTU 10 MW reference turbine [21]. A linear eigenvalue buckling analysis is performed using a 3D finite element model and the program ABAQUS. In contrast to the DTU approach solid elements are used instead of shell elements to account for variations in wall thickness. The blade is divided into segments with a length of approximately 1.2 times the midsection's local chord length. Kinematic coupling constraints are applied to reference nodes at both ends of the segment. One reference node is fixed, the other is loaded such that the midsection is loaded by the ultimate loads resulting from the load calculation (section 2.5). Safety factors are applied according to IEC 61400-1 and summarized in table 14.

Table 14: Safety factors for stability

safety factor	value	standard
γ_f	1.35	IEC 61400
γ_m	1.1	IEC 61400
γ_n	1.0	IEC 61400

2.9 Critical Deflection

Critical deflection of the blade tip is checked as proposed by Resor [6]. Based on the information provided by Jonkman et al. [5], a tower clearance of 10.5 m is calculated for the NREL 5 MW wind turbine. Taking safety factors into account, an allowable blade tip deflection of 7.07 m remains. The out-of-blade deflection of the blade tip is recorded for all simulations. Its extreme value is checked against the allowable blade tip deflection.

Table 15: Safety factors for critical deflection

safety factor	value	standard
γ_f	1.35	IEC 61400
γ_m	1.2	IEC 61400
γ_n	1.0	IEC 61400

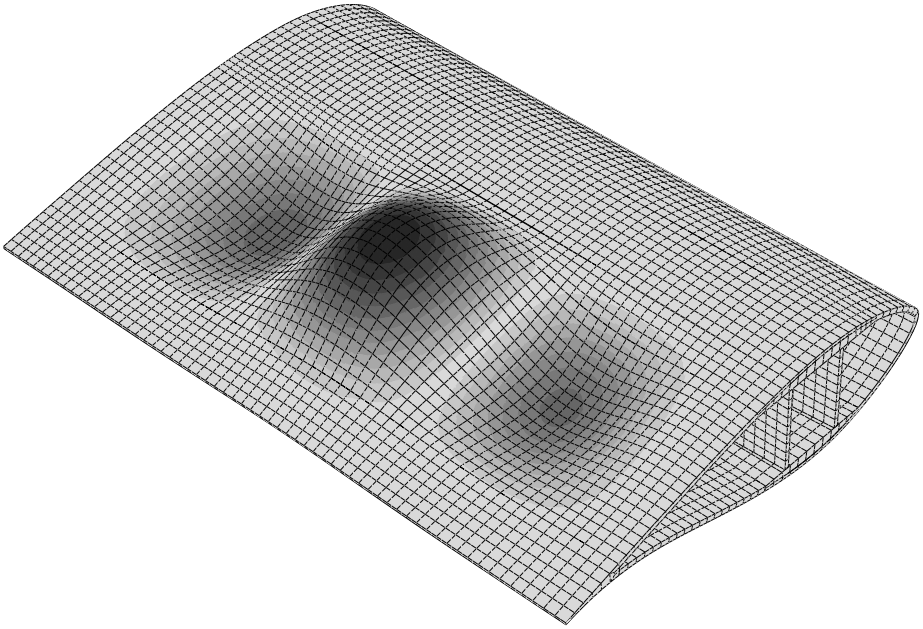

Figure 14: Typical first buckling mode shape

3 Results

The structural design of the presented wood-CFRP rotor blade differs from conventional blade design. Still, the resulting elastic properties and loads are pretty similar to those of the conventional reference blade.

3.1 Wood-CFRP Blade Model

A final design could be reached that meets all the required design criteria. Ultimate strength and buckling resistance showed to be the most critical design drivers.

3.1.1 Internal Structure

Figure 15 plots the most relevant resulting structural parameters over the spanwise position of the blade. The wall thickness at leading and trailing edge is decreasing from 100 mm at the root to 35 mm towards the tip. The spar enforcement thickness exceeds wall thickness at most of the cross sections and reaches its maximum of 160 mm at 23.3% blade length. Flapwise stiffness is enforced by spar caps that reach from the blade root to 83.3% blade length. The highest spar cap thickness of 39 mm is reached at 23.3% blade length. One shear web of 40 mm thickness exceeds from 11.1 % blade length to the blade tip. Another

shear web of 40 mm thickness reaches from 11.1% blade length to 63.3% blade length. Exemplary cross sections are shown in the appendix.

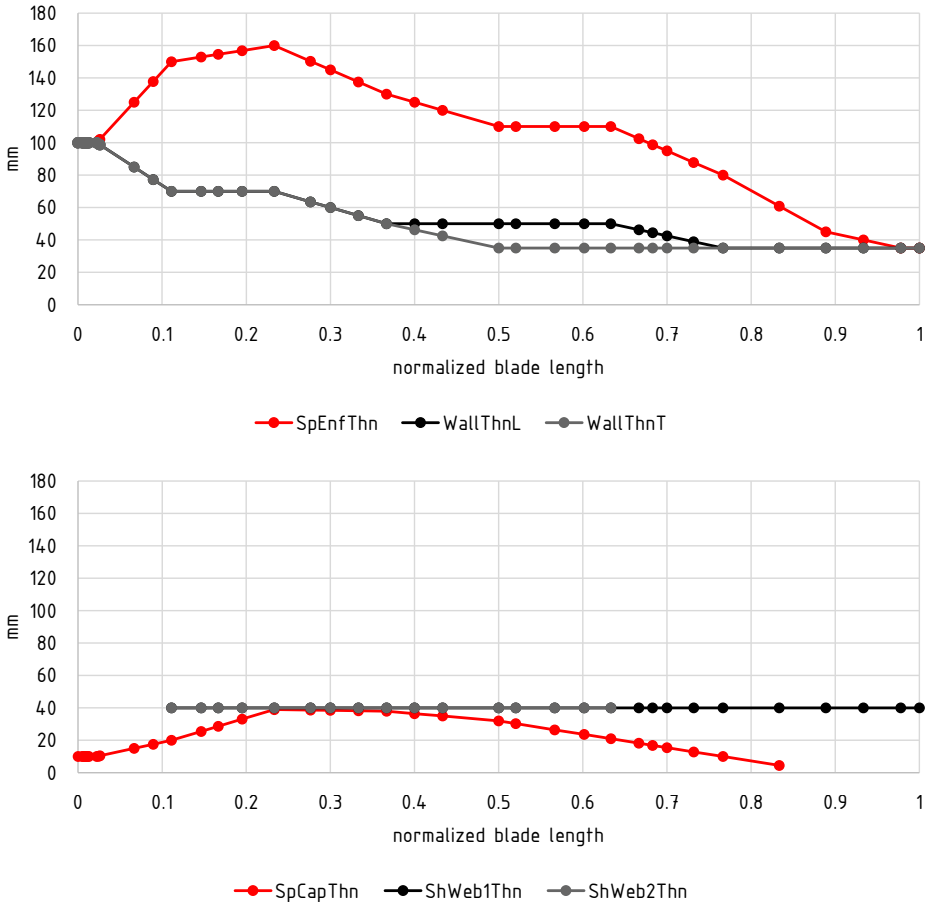

Figure 15: internal structure

3.1.2 Ultimate Strength

Ultimate normal strength in the spar region (LVL) is the most critical dimensioning parameter. Figure 16 shows that utilization of material strength is close to 100% for all cross sections except the blade tip section. Utilization of the spar cap material is at around 30%.

3.1.3 Fatigue Strength

Assumptions for the analysis of fatigue strength of wood are very conservative. Still, fatigue strength is not a dimensioning parameter for neither wood nor CFRP. As can be seen in figure 16 fatigue utilization of wood is below 80%

for all cross sections. Fatigue utilization of CFRP is below 30% for all cross sections.

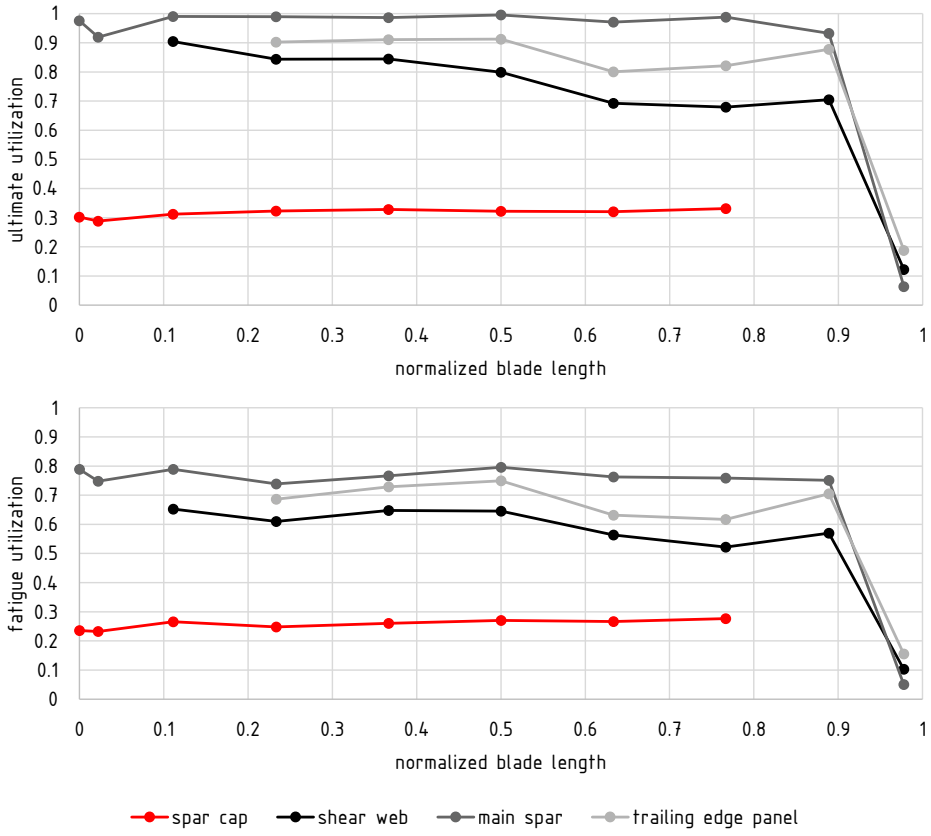

Figure 16: Ultimate and fatigue load utilization

3.1.4 Stability

Stability of the trailing edge panel is a dimensioning criterion for the presented wood-CFRP blade design and requires an adequate wall thickness. Figure 17 plots the ratio of the combined safety factor to the load factor for the first buckling mode of the respective element.

3.1.5 Critical Deflection

Table 16 shows the ultimate tip deflections of all three blades. In all situations out-of-plane tip deflection is less than the allowable tip deflection of 7.07 m .

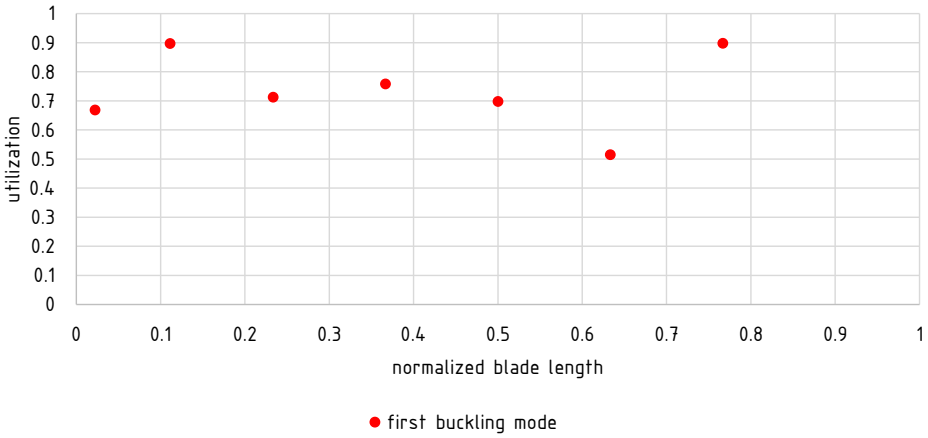

Figure 17: Buckling utilization

Table 16: Tip deflection

deflection	min m	max m
out-of-plane	-2.13	5.04
in-plane	-4.61	3.39

3.2 Comparison to Conventional Reference Blade Model

The wood-CFRP blade model is compared against a conventional blade model with respect to elastic properties, loads, and bill of materials.

3.2.1 Conventional Reference Blade Model

The wood-CFRP blade model shall be compared to the conventional blade model designed by Resor [6]. This blade model has been designed for the NREL 5 MW wind turbine and onshore conditions (IEC IB). Next to meeting the basic IEC design load criteria, Resor's objective was to match the overall blade mass and spanwise trends of elastic properties that were given with the documentation of the reference turbine.

The reference blade geometry is the same as for the wood-CFRP blade as explained in section 2.1.

The reference blade model is designed as a conventional blade with half shells and shear webs made of glass fiber, foam, and epoxy combined in an infusion process. The blade is enforced with spar caps made of carbon prepregs. Blade root hardware, lightning protection and coating are not considered.

3.2.2 Elastic Properties and Loads

The wood-CFRP blade is compared to the conventional blade in terms of edgewise and flapwise stiffness at 38 cross sections. For both blade models edgewise and flapwise stiffness are given with respect to the elastic axes of the respective cross section. This comparison shows that flapwise stiffness of the wood-CFRP blade model is in good agreement with the flapwise stiffness of the conventional blade model. In comparison with the conventional blade model the wood-CFRP blade is slightly stiffer towards the root section and less stiff towards the blade tip.

In terms of edgewise stiffness, the comparison shows that the wood-CFRP blade is stiffer than the reference blade in most of the cross section. This is due to the relatively high wall thickness at the leading and trailing edge regions that is needed for buckling resistance.

Overall blade mass of the wood-CFRP blade is 18 500 kg, which is 104.5% of the reference blade mass. The comparison of the distributed blade mass density shows that the wood-CFRP blade is significantly lighter around the blade root section but slightly heavier from 10% span onward.

The first three natural frequencies of the wood-CFRP blade and the reference blade are given in table 17. Natural frequencies are calculated with BModes using the same settings for both blade models.

Table 17: Eigenfrequencies

	1st flapwise f Hz	1st edgewise f Hz	2nd flapwise f Hz
wood-CFRP	1.02	1.44	2.77
reference	0.95	1.10	2.91

Ultimate loads are similar for the wood-CFRP blade and the reference blade. Deviations in the magnitude of the ultimate resulting bending moment are less than 10% for all cross section and less than 3% for the outer half of the rotor blade. The spanwise ultimate resulting bending moment is shown in figure 19.

As compared to the reference blade DEL ($n_{ref} = 10^7$, $m = 18$) of the wood-CFRP blade are around 20% higher in edgewise direction. This increase in edgewise fatigue loading is due to the higher edgewise stiffness and the slightly higher blade mass. Fatigue loads in flapwise direction are similar for the reference blade and for the wood-CFRP blade.

3.2.3 Bill of Materials

Comparing wood-CFRP blade and reference blade in terms of bill of materials shows that GFRP and GFRP sandwich materials of the reference blade can be fully substituted by LVL (see table 18). Additionally, the amount of carbon prepreg can be reduced by 20%.

The bill of materials do not include cutoff and refuse.

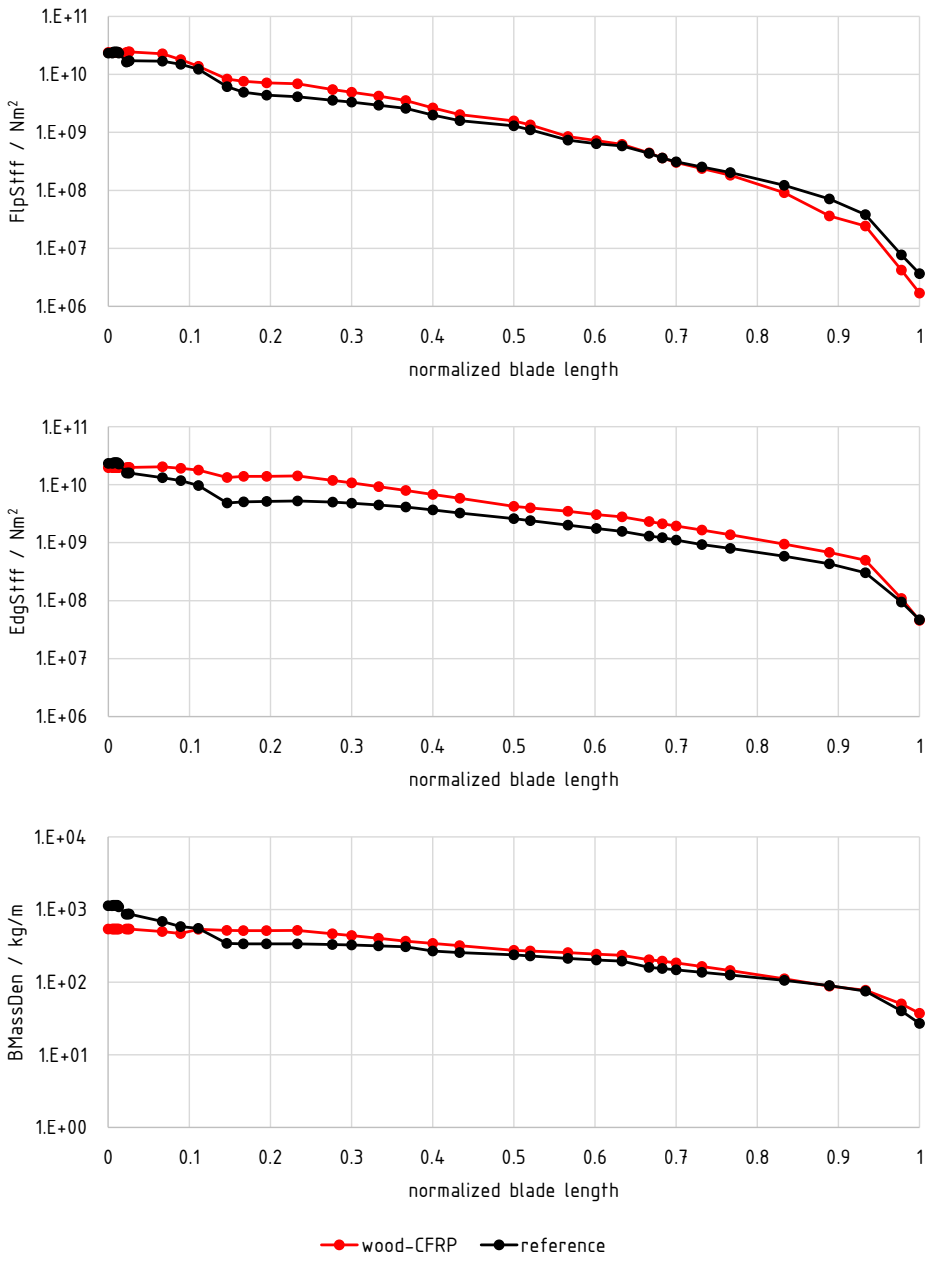

Figure 18: Stiffness and mass distribution

Under the assumption that LVL is less expensive and less energy intensive than GFRP and foam, it seems likely that a wood-CFRP blade has less net material cost and a better environmental performance than the reference blade.

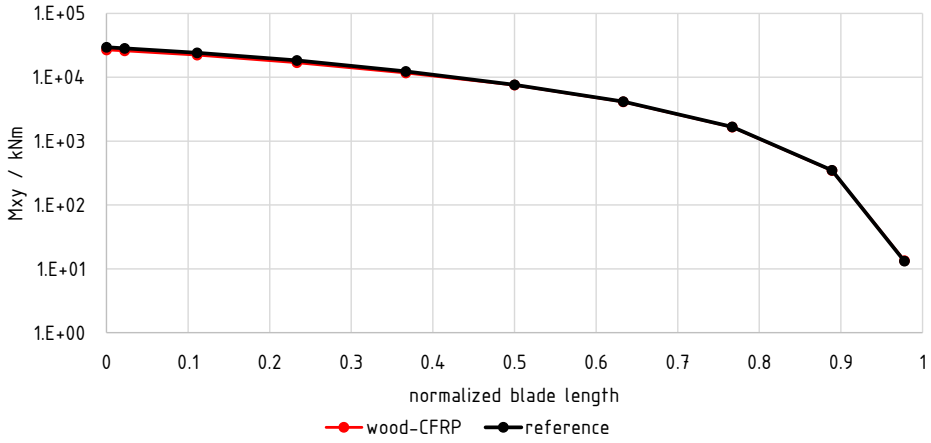

Figure 19: Ultimate resulting bending moment

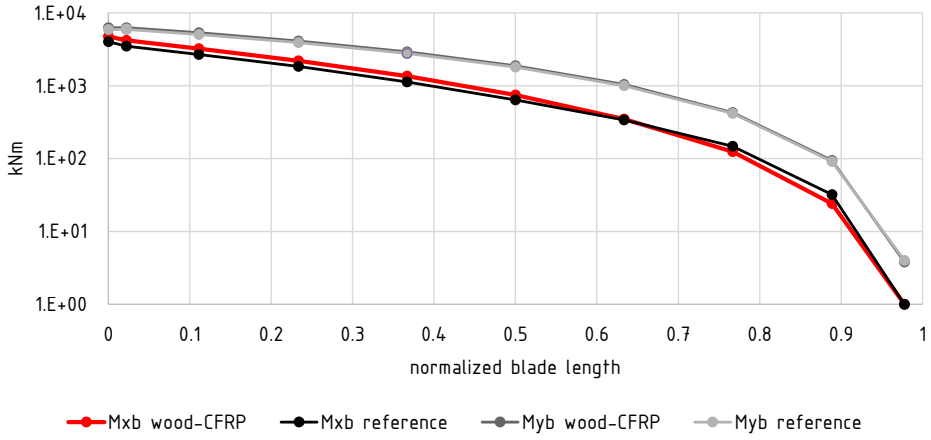

Figure 20: Edgewise and flapwise fatigue loads (DEL)

Table 18: Bill of materials

material		mass kg	share of total %
wood-CFRP		**18511**	**100**
LVL	LVL Uniax	10572	57.1
	LVL Biax (0/90)	3882	21.0
	LVL Biax (-45/45)	1590	8.6
carbon prepreg	Newport 307 Prepreg (incl. resin)	2467	13.0
reference		**17700**	**100**
glass fiber	E-LT-55 Uni fiber	2439	13.8
	Saertex DB fiber	2811	15.9
foam		3855	21.8
gelcoat		29	0.2
total resin		5481	31.0
carbon prepreg	Newport 307 Prepreg (incl. resin)	3085	17.4

4 Conclusion

It is possible to design a wood-CFRP wind turbine blade for the NREL 5 MW wind turbine under onshore conditions according to IEC 61400-1. The overall blade mass and beam elastic properties are similar to a conventional blade.

A comparison of the bill of materials of both the wood-CFRP blade and the reference blade indicates an advantage for the wood-CFRP blade in terms of net material cost and environmental performance. Still, material costs will be highly dependent on the rate of cutoff.

The overall advantage of the presented blade design approach is highly dependent on the feasibility and economic competitiveness of the manufacturing process. An analysis of these open points should be the focus of future work.

Annotation

This work was funded by EKSH and was conducted in cooperation with PHI Blades GmbH.

References

[1] M. F. Ashby. *Materials Selection in Mechanical Design*. Butterworth-Heinemann, 2005.

[2] E. Hau. *Wind Turbines: Fundamentals, Technologies, Application, Economics*. Springer, 2013.

[3] M. Gougeon. *The Gougeon Brothers on Boat Building: Wood and West System Materials*. Gougeon Brothers Inc., 2005.

[4] P. Brønsted, H. Lilholt, and A. Lystrup. Composite materials for wind power turbine blades. *Annual Review of Materials Research*, 35:505–538, 2005.

[5] J. M. Jonkman, S. Butterfield, W. Musial, and G. Scott. Definition of a 5-MW reference wind turbine for offshore system development. Technical report, National Renewable Energy Laboratory, 2009.

[6] B. R. Resor. Definition of a 5MW/61.5m wind turbine blade reference model. Technical report, Sandia National Laboratories, 2013.

[7] W. A. Beerschoten, D. M. Carradine, and A. Carr. Development of constitutive model for laminated veneer lumber using digital image correlation technique. *Wood Science and Technology*, 48:755–772, 2014.

[8] Nelson Pine. NPIL/LVL 04. Technical report, Nelson Pine Industries Ltd, 2010.

[9] Pollmeier. PM-003-2015: laminated veneer lumber made of beech. Technical report, Pollmeier Furnierwerkstoffe GmbH, 2015.

[10] DIBt. Z-9.1-842. Technical report, Deutsches Institut für Bautechnik, 2015.

[11] DIBt. Z-9.1-847. Technical report, Deutsches Institut für Bautechnik, 2014.

[12] J. P. Blasques, R. D. Bitsche, V. Fedorov, and B. S. Lazarov. Accuracy of an efficient framework for strctural analysis of wind turbine blades. *Wind Energy*, 2015.

[13] G. Bir. User's guide to BModes (software for computing rotating beam coupled modes). Technical report, National Renewable Energy Laboratory, 2005.

[14] J. M. Jonkman and M. L. Buhl Jr. FAST user's guide. Technical report, National Renewable Energy Laboratory, 2005.

[15] J. M. Jonkman and L Kilcher. TurbSim user's guide: Version 1.06.00. Technical report, National Renewable Energy Laboratory, 2012.

[16] IEC 61400-1:2005: Wind turbines - Part 1: Design requirements.

[17] G. F. Hayman. MExtremes manual: Version 1.00. Technical report, National Renewable Energy Laboratory, 2015.

[18] G. F. Hayman and M. Buhl. MLife user's guide: Version 1.00. Technical report, National Renewable Energy Laboratory, 2012.

[19] GL Guideline for the Certification of Wind Turbines: Edition 2010.

[20] P. W. Bonfield and M. P. Ansell. Fatigue properties of wood in tension, compression and shear. *Journal of Materials Science*, 26:4765–4773, 1991.

[21] C. Bak, F. Zahle, R. Bitsche, K. Taeseong, A. Yde, L. C. Henriksen, A. Natarajan, and M. H. Hansen. Description of the DTU 10 MW reference wind turbine. Technical report, Technical University of Danmark, 2013.

Appendix 1: FAST Blade Input File

```
---------------------- FAST INDIVIDUAL BLADE FILE ------------------------------
Blade Data created from BECAS
---------------------- BLADE PARAMETERS ----------------------------------------
38              NBlInpSt    - Number of blade input stations (-)
1.5             BldFlDmp(1) - Blade flap mode #1 structural damping
1.5             BldFlDmp(2) - Blade flap mode #2 structural damping
1.5             BldEdDmp(1) - Blade edge mode #1 structural damping
---------------------- BLADE ADJUSTMENT FACTORS --------------------------------
1               FlStTunr(1) - Blade flapwise modal stiffness tuner, 1st mode (-)
1               FlStTunr(2) - Blade flapwise modal stiffness tuner, 2st mode (-)
1               AdjBlMs     - Factor to adjust blade mass density (-)
1               AdjFlSt     - Factor to adjust blade flap stiffness (-)
1               AdjEdSt     - Factor to adjust blade edge stiffness (-)
---------------------- DISTRIBUTED BLADE PROPERTIES ----------------------------
BlFract  PitchAxis StrcTwst    BMassDen    FlpStff       EdgStff
(-)      (-)       (deg)       (kg/m)      (Nm^2)        (Nm^2)
0.00000  0.000     1.2782e+01  5.3753e+02  2.39071e+10   1.96014e+10
0.00488  0.000     1.2782e+01  5.3753e+02  2.39071e+10   1.96014e+10
0.00650  0.000     1.2798e+01  5.3752e+02  2.39070e+10   1.96022e+10
0.00813  0.000     1.2794e+01  5.3754e+02  2.39075e+10   1.96027e+10
0.00976  0.000     1.2796e+01  5.3753e+02  2.39067e+10   1.96027e+10
0.01138  0.000     1.2798e+01  5.3754e+02  2.39087e+10   1.96028e+10
0.01301  0.000     1.2799e+01  5.3754e+02  2.39087e+10   1.96025e+10
0.02222  0.000     1.2782e+01  5.3753e+02  2.39071e+10   1.96014e+10
0.02439  0.002     1.3269e+01  5.3697e+02  2.42318e+10   1.97802e+10
0.02602  0.003     1.3241e+01  5.3645e+02  2.44532e+10   1.99024e+10
0.06667  0.038     8.5368e+00  4.9691e+02  2.26082e+10   2.03379e+10
0.08943  0.058     2.5828e+01  4.6741e+02  1.79671e+10   1.91636e+10
0.11111  0.077     1.7982e+01  5.3299e+02  1.37302e+10   1.78222e+10
0.14634  0.107     1.6361e+01  5.1441e+02  8.34178e+09   1.32956e+10
0.16667  0.125     1.6774e+01  5.1130e+02  7.62481e+09   1.39247e+10
0.19512  0.125     1.6847e+01  5.1049e+02  7.13988e+09   1.39195e+10
0.23333  0.125     1.6336e+01  5.1487e+02  6.87892e+09   1.42057e+10
0.27642  0.125     1.5351e+01  4.6375e+02  5.46445e+09   1.18284e+10
0.30000  0.125     1.5000e+01  4.3815e+02  4.92399e+09   1.07488e+10
0.33333  0.125     1.4484e+01  4.0155e+02  4.23475e+09   9.20823e+09
0.36667  0.125     1.3560e+01  3.6676e+02  3.53121e+09   7.92850e+09
0.40000  0.125     1.1456e+01  3.4150e+02  2.64514e+09   6.76509e+09
0.43333  0.125     9.9741e+00  3.1796e+02  2.01691e+09   5.82326e+09
0.50000  0.125     8.7875e+00  2.7454e+02  1.57358e+09   4.24048e+09
0.52033  0.125     7.9091e+00  2.6771e+02  1.34391e+09   3.95906e+09
0.56667  0.125     5.3659e+00  2.5480e+02  8.49752e+08   3.46871e+09
0.60163  0.125     4.5782e+00  2.4333e+02  7.24442e+08   3.05108e+09
0.63333  0.125     4.1087e+00  2.3362e+02  6.22605e+08   2.77782e+09
0.66667  0.125     3.1172e+00  2.0370e+02  4.42017e+08   2.30572e+09
0.68293  0.125     2.5558e+00  1.9426e+02  3.60786e+08   2.11173e+09
0.70000  0.125     2.1540e+00  1.8365e+02  3.03091e+08   1.93682e+09
0.73171  0.125     1.9199e+00  1.6490e+02  2.38673e+08   1.64468e+09
0.76667  0.125     2.0731e+00  1.4488e+02  1.82645e+08   1.36431e+09
0.83333  0.125     1.5666e+00  1.1084e+02  9.08531e+07   9.39604e+08
0.88889  0.125     1.3683e+00  8.8100e+01  3.62654e+07   6.77792e+08
0.93333  0.125     8.8147e-01  7.7358e+01  2.41726e+07   4.95098e+08
0.97778  0.125     1.8515e+00  5.0285e+01  4.23589e+06   1.09262e+08
1.00000  0.125     1.8136e+00  3.7283e+01  1.69399e+06   4.55639e+07
---------------------- BLADE MODE SHAPES ---------------------------------------
0.0910          BldFl1Sh(2) - Flap mode 1, coeff of x^2
1.9461          BldFl1Sh(3) -            , coeff of x^3
-3.9985         BldFl1Sh(4) -            , coeff of x^4
5.1938          BldFl1Sh(5) -            , coeff of x^5
-2.2324         BldFl1Sh(6) -            , coeff of x^6
-1.6075         BldFl2Sh(2) - Flap mode 2, coeff of x^2
8.1314          BldFl2Sh(3) -            , coeff of x^3
-27.7253        BldFl2Sh(4) -            , coeff of x^4
36.1705         BldFl2Sh(5) -            , coeff of x^5
-13.9690        BldFl2Sh(6) -            , coeff of x^6
1.0581          BldEdgSh(2) - Edge mode 1, coeff of x^2
-0.8400         BldEdgSh(3) -            , coeff of x^3
2.3921          BldEdgSh(4) -            , coeff of x^4
-2.2255         BldEdgSh(5) -            , coeff of x^5
0.6152          BldEdgSh(6) -            , coeff of x^6
```

Appendix 2: Cross Sections

Cross Section 1

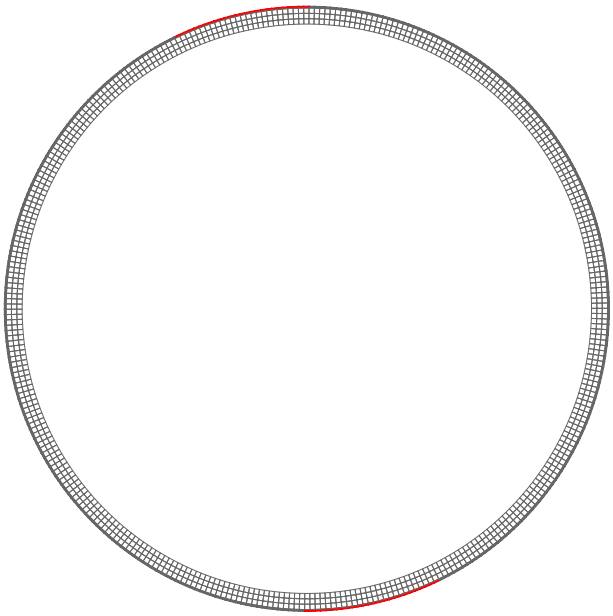

Cross Section 8

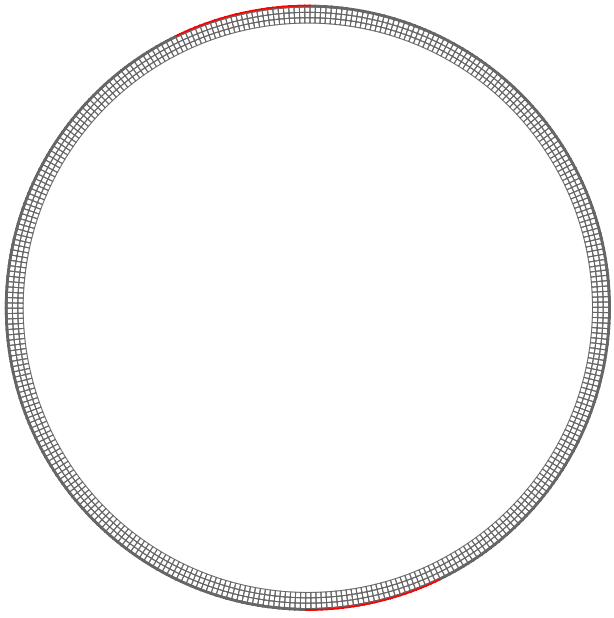

Cross Section 13

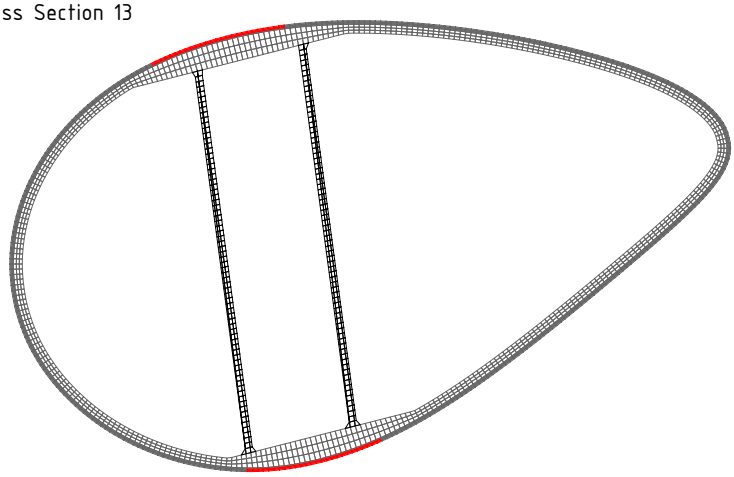

Cross Section 17

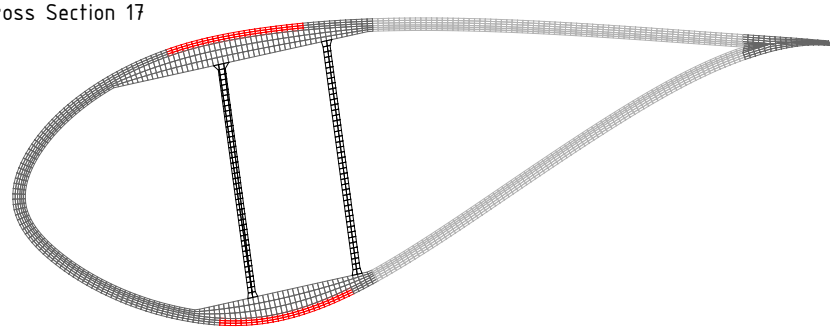

Cross Section 21

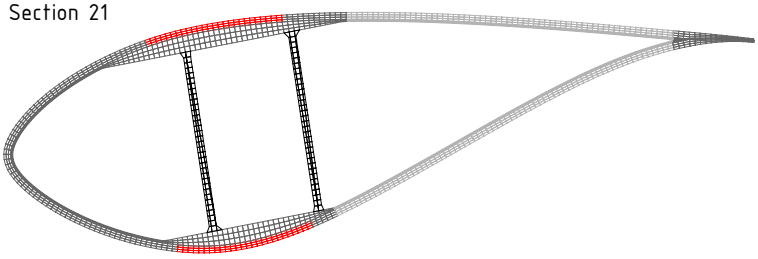

Cross Section 24

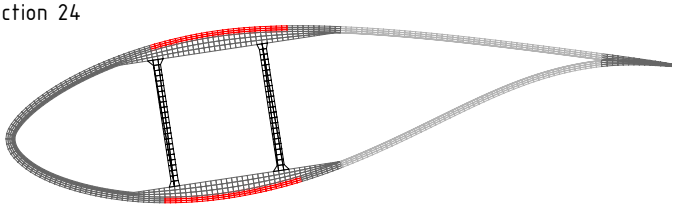

Cross Section 28

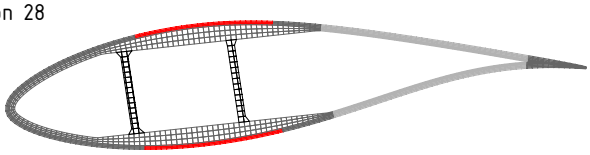

Cross Section 33

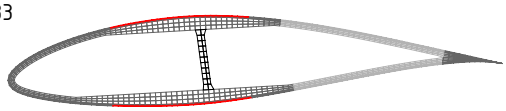

Cross Section 35

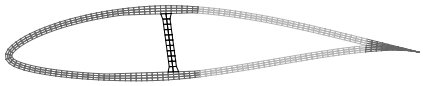

Cross Section 37

Appendix 3: Loads

Table 19: Cross Section 1

		F_x kN	F_y kN	F_z kN	M_x kNm	M_y kNm	F_z kNm	F_{xy} kN	M_{xy} kNm
F_x	min	-697	50	-270	927	-20480	489	699	20500
	max	704	-163	-276	4814	20453	-563	723	21011
F_y	min	496	-374	842	9855	18320	-367	621	20802
	max	52	314	930	-7480	1507	-145	318	7631
F_z	min	492	1	-295	2568	20966	-471	492	21122
	max	198	-35	1501	576	3299	-219	201	3349
M_x	min	200	302	1145	-7840	5177	-266	362	9396
	max	492	-374	830	9885	18050	-365	618	20579
M_y	min	-663	63	-271	802	-21735	749	666	21750
	max	659	-106	-275	5742	26244	-661	668	26865
M_z	min	657	-112	-276	5894	26217	-664	666	26871
	max	-662	64	-270	772	-21708	751	665	21722
F_{xy}	min	686	-362	815	9393	25201	-373	776	26895
M_{xy}	max	686	-362	815	9393	25201	-373	776	26895

Table 20: Cross Section 8

		F_x kN	F_y kN	F_z kN	M_x kNm	M_y kNm	F_z kNm	F_{xy} kN	M_{xy} kNm
F_x	min	-685	-110	-260	5220	-18860	486	694	19569
	max	746	-192	813	3321	25645	-373	770	25859
F_y	min	169	-263	967	6698	1309	-152	313	6824
	max	257	340	916	-8904	9994	-143	426	13385
F_z	min	482	100	-285	-1974	20358	-473	493	20453
	max	198	9	1485	-155	3074	-218	198	3078
M_x	min	257	340	916	-8904	9994	-143	426	13385
	max	149	-256	1086	7386	-1766	-134	296	7594
M_y	min	-658	-93	-262	5470	-20115	747	665	20846
	max	673	33	-267	-114	25961	-663	673	25961
M_z	min	672	29	-267	-26	25961	-664	673	25961
	max	-658	-92	-261	5435	-20102	750	664	20823
F_{xy}	min	746	-192	813	3321	25645	-373	770	25859
M_{xy}	max	746	-192	813	3321	25645	-373	770	25859

Table 21: Cross Section 13

		F_x kN	F_y kN	F_z kN	M_x kNm	M_y kNm	F_z kNm	F_{xy} kN	M_{xy} kNm
F_x	min	-647	-203	-220	5823	-14702	471	678	15813
	max	741	-93	792	400	21695	-365	746	21698
F_y	min	136	-225	1041	6238	-1931	-132	263	6529
	max	465	325	912	-7964	15188	-186	568	17149
F_z	min	482	104	-246	-3135	17483	-478	493	17761
	max	183	22	1403	-297	2012	-216	185	2033
M_x	min	457	323	913	-7985	15093	-181	560	17075
	max	-632	-186	-224	6350	-15957	729	659	17174
M_y	min	-635	-187	-224	6346	-16025	731	662	17235
	max	694	61	-232	-2021	22127	-663	697	22219
M_z	min	694	58	-233	-1963	22127	-664	696	22213
	max	-636	-186	-223	6325	-16025	735	662	17228
F_{xy}	min	741	-93	792	400	21695	-365	746	21698
M_{xy}	max	734	-93	791	414	21735	-362	740	21739

Table 22: Cross Section 17

		F_x kN	F_y kN	F_z kN	M_x kNm	M_y kNm	F_z kNm	F_{xy} kN	M_{xy} kNm
F_x	min	-647	-203	-220	5823	-14702	471	678	15813
	max	741	-93	792	400	21695	-365	746	21698
F_y	min	136	-225	1041	6238	-1931	-132	263	6529
	max	465	325	912	-7964	15188	-186	568	17149
F_z	min	482	104	-246	-3135	17483	-478	493	17761
	max	183	22	1403	-297	2012	-216	185	2033
M_x	min	457	323	913	-7985	15093	-181	560	17075
	max	-632	-186	-224	6350	-15957	729	659	17174
M_y	min	-635	-187	-224	6346	-16025	731	662	17235
	max	694	61	-232	-2021	22127	-663	697	22219
M_z	min	694	58	-233	-1963	22127	-664	696	22213
	max	-636	-186	-223	6325	-16025	735	662	17228
F_{xy}	min	741	-93	792	400	21695	-365	746	21698
M_{xy}	max	734	-93	791	414	21735	-362	740	21739

Table 23: Cross Section 21

		F_x kN	F_y kN	F_z kN	M_x kNm	M_y kNm	F_z kNm	F_{xy} kN	M_{xy} kNm
F_x	min	-437	-130	-119	2916	-7812	359	456	8339
	max	625	4	-130	-260	11429	-506	625	11432
F_y	min	-46	-151	729	3094	-2861	-73	158	4214
	max	224	195	636	-3370	4801	-147	297	5865
F_z	min	490	47	-134	-947	9854	-419	492	9899
	max	66	10	956	15	16	-146	67	22
M_x	min	224	195	636	-3370	4801	-147	297	5865
	max	-33	-144	733	3145	-2788	-46	148	4202
M_y	min	-437	-130	-119	2916	-7812	358	456	8339
	max	549	-37	550	157	11721	-400	550	11722
M_z	min	625	2	-130	-231	11436	-507	625	11438
	max	-436	-129	-118	2897	-7806	359	455	8326
F_{xy}	min	625	4	-130	-260	11429	-506	625	11432
M_{xy}	max	549	-37	550	157	11721	-400	550	11722

Table 24: Cross Section 24

		F_x kN	F_y kN	F_z kN	M_x kNm	M_y kNm	F_z kNm	F_{xy} kN	M_{xy} kNm
F_x	min	-337	-89	-79	1515	-4833	213	348	5065
	max	487	-35	-87	369	6831	-346	488	6841
F_y	min	-89	-114	542	1828	-2476	-42	145	3078
	max	92	131	514	-1651	679	-136	160	1785
F_z	min	416	4	-90	-75	6133	-309	416	6134
	max	22	3	706	49	-314	-103	22	318
M_x	min	204	129	478	-1713	3195	-126	242	3626
	max	-78	-110	544	1882	-2381	-18	135	3035
M_y	min	-336	-89	-79	1516	-4833	212	348	5065
	max	466	-52	412	575	7517	-327	469	7539
M_z	min	487	-35	-87	371	6831	-346	488	6841
	max	-335	-87	-78	1488	-4810	215	346	5035
F_{xy}	min	487	-36	-87	377	6831	-346	488	6841
M_{xy}	max	466	-52	412	575	7517	-327	469	7539

Table 25: Cross Section 28

		F_x kN	F_y kN	F_z kN	M_x kNm	M_y kNm	F_z kNm	F_{xy} kN	M_{xy} kNm
F_x	min	-243	-55	-45	636	-2542	113	249	2620
	max	357	-60	272	598	4073	-224	362	4117
F_y	min	-113	-80	351	929	-1696	7	138	1934
	max	48	82	337	-746	224	-80	94	779
F_z	min	301	-22	-52	220	3164	-188	302	3172
	max	-7	0	454	30	-377	-60	7	378
M_x	min	45	80	296	-751	244	-66	92	790
	max	-113	-80	351	929	-1696	7	138	1934
M_y	min	-243	-55	-46	638	-2543	112	249	2622
	max	357	-59	271	581	4077	-226	362	4118
M_z	min	337	-45	260	424	3835	-235	340	3859
	max	-243	-54	-45	630	-2539	114	249	2616
F_{xy}	min	357	-62	275	622	4065	-222	362	4112
M_{xy}	max	357	-59	271	581	4077	-226	362	4118

Table 26: Cross Section 33

		F_x kN	F_y kN	F_z kN	M_x kNm	M_y kNm	F_z kNm	F_{xy} kN	M_{xy} kNm
F_x	min	-146	-32	-20	222	-961	50	150	986
	max	233	-42	144	275	1632	-124	237	1655
F_y	min	-107	-51	182	348	-765	13	119	841
	max	12	41	154	-257	54	-34	43	263
F_z	min	180	-19	-23	126	1192	-93	181	1198
	max	-23	-2	234	27	-255	-30	23	256
M_x	min	12	41	154	-257	54	-34	43	263
	max	-107	-51	182	348	-765	13	119	841
M_y	min	-125	-31	187	250	-969	31	128	1001
	max	233	-40	143	264	1632	-124	237	1653
M_z	min	213	-28	139	176	1485	-131	214	1495
	max	-145	-31	-20	215	-952	51	148	976
F_{xy}	min	233	-44	146	288	1628	-121	237	1653
M_{xy}	max	233	-42	144	277	1632	-123	237	1656

Table 27: Cross Section 35

		F_x kN	F_y kN	F_z kN	M_x kNm	M_y kNm	F_z kNm	F_{xy} kN	M_{xy} kNm
F_x	min	-67	-17	71	58	-227	13	69	234
	max	107	-18	57	58	340	-46	109	345
F_y	min	-53	-22	69	67	-164	2	57	177
	max	7	16	73	-48	18	-14	17	52
F_z	min	76	-9	-7	28	234	-31	76	236
	max	-21	-4	88	15	-84	-8	22	85
M_x	min	7	16	73	-48	18	-14	17	52
	max	-50	-20	71	70	-170	8	54	184
M_y	min	-65	-8	73	34	-233	11	66	236
	max	107	-19	57	59	341	-46	109	346
M_z	min	96	-11	55	35	306	-49	97	308
	max	-56	-16	69	51	-171	17	58	178
F_{xy}	min	107	-20	57	61	340	-46	109	346
M_{xy}	max	107	-19	57	59	341	-46	109	346

Table 28: Cross Section 37

		F_x kN	F_y kN	F_z kN	M_x kNm	M_y kNm	F_z kNm	F_{xy} kN	M_{xy} kNm
F_x	min	-14	-2	11	2	-10	2	14	10
	max	18	-3	9	2	13	-4	18	13
F_y	min	-10	-4	12	3	-7	2	11	8
	max	0	2	9	-2	0	-1	2	2
F_z	min	6	0	-1	0	4	-2	6	4
	max	-5	-1	14	1	-4	-1	6	4
M_x	min	0	2	9	-2	0	-1	2	2
	max	-10	-4	12	3	-7	2	11	8
M_y	min	-14	-2	11	2	-10	2	14	10
	max	18	-3	9	2	13	-4	18	13
M_z	min	16	-2	9	1	12	-6	16	12
	max	-14	-2	11	2	-10	2	14	10
F_{xy}	min	18	-3	9	2	13	-4	18	13
M_{xy}	max	18	-3	9	2	13	-4	18	13